

## Modelling and Simulation of the Testbed for a Pitch-Roll Wrist Prototype Based on Spherical Cam-Rollers

Xiao Qing Ma<sup>1</sup>, Vikram Chopra<sup>1</sup>, Jorge Angeles<sup>1</sup>, Martin Asger Haugaard<sup>2</sup>

<sup>1</sup> *Department of Mechanical Engineering & Centre for Intelligent Machines, McGill University, Montreal, Canada*  
email: { xqma, vikram, angeles } @cim.mcgill.ca

<sup>2</sup> *Department of Mechanical Engineering, Technical University of Denmark, Nils Koppels Alle, Denmark*  
email: mah@mek.dtu.dk

---

### Abstract

Robotic wrists with light weight and high stiffness are needed for accurate manipulation tasks. A prototype of a novel two-degree-of-freedom wrist based on spherical cam-rollers was developed at McGill University with the aim of replacing bevel gears in robotic manipulators, as these gears bring about backlash and Coulomb friction, that mars robot performance. In order to identify the stiffness and damping parameters of the prototype, a testbed was designed and fabricated. This paper reports the design and formulation of a mathematical model of this testbed, on which the identification procedure will be implemented.

**Keywords:** cam-roller pair, pitch-roll wrist, testbed, mathematical model, parameter identification

---

### Modélisation et simulation d'un banc d'essai pour un poignet tangage-roulis construit à base de mécanismes à cames et roulements

#### Résumé

Les manipulations précises exigent des poignets robotiques légers et rigides. L'Université McGill a mis au point un prototype novateur de poignet à deux degrés de liberté basé sur des transmissions à cames et rouleaux. L'élimination des engrenages coniques des manipulateurs robotiques qui produisent du jeu et du frottement de Coulomb permettra d'améliorer la performance des robots. Les auteurs ont conçu un banc d'essai afin de déterminer les paramètres de raideur et d'amortissement du poignet. Cet article présente le modèle mathématique du banc d'essai mis au point par les auteurs pour déterminer les paramètres de raideur et d'amortissement du poignet.

**Mots-clé:** cames, poignet tangage-roulis, banc d'essai, modèle mathématique, identification des paramètres

---

## 1 INTRODUCTION

Robotic wrists are commonly used in manipulators for applications that require a large dexterous workspace [1]. Epicyclic bevel gear trains are common architectures for wrists, due to their relative simplicity and compactness. Rosheim [1] developed a large survey on mechanisms commonly used in different types of robotic wrists. In the last two decades, several studies have been conducted on the structural synthesis of spherical wrist mechanisms. Tsai [2] introduced the canonical graph of a bevel-gear robotic wrist mechanisms to avoid the pseudoisomorphic problem, having established a complete atlas of bevel-gear wrist mechanisms with up to eight links. Hsu et al. [3] developed an efficient methodology for structural synthesis of all the three-degree-of-freedom (dof) robotic wrist mechanisms with  $N$  links from the catalog of two-dof geared kinematic chains with  $N - 1$  links. In fact, as a robotic wrist is to be attached to a moving arm, design criteria for such wrists are compactness, accuracy, light weight, high mechanical stiffness, and low backlash. However, the conventional mechanical transmissions based on gears, mentioned above, entail drawbacks in robotics applications, such as backlash, unavoidable friction, and low stiffness.

Researchers have reported efforts to design wrists with different approaches in order to improve their performance. Wiitala and Stanisic [4] proposed an overconstrained mechanism with a symmetric spherical eight-bar linkage, whose significant achievement is a hemisphere-singularity-free workspace. A three-dof parallel spherical wrist was designed by Gosselin et al., the “Agile Eye” [5], employing both revolute and spherical joints. Spherical Stephenson mechanisms combined with cam-rollers were proposed by Hernandez et al. [6] to implement a pitch-roll wrist.

Recently, a two-dof gearless pitch-roll wrist (PRW) [7] based on spherical cam-rollers was developed at McGill University; its physical prototype is shown in Fig. 1. The mechanism is composed of: two sets of input conical roller-carriers, one outside of the carrier and visible in Fig. 1, the other inside and hidden in the same photograph; each roller set drives one of two coaxial, conjugate, multi-lobe spherical cams, one external and visible in Fig. 1, the other internal and hidden in the same figure. The rollers from the two roller-carriers drive the double-cam assembly to produce a differential motion. The two cams work alternatively to ensure a positive motion. The wrist has the advantages of high stiffness and low backlash, inherent to cam transmissions. Moreover, the wrist offers an unlimited workspace. The downside of the prototype is its size and weight. Actually, the latter is a consequence of the former, which was dictated by budgetary constraints. Indeed, the size was determined by the smallest possible rollers found in the market for non-precision bearings. Using the latter would have substantially increased the prototype cost.

The paper begins with a description of the testbed, which is designed to conduct tests on the performance of the above-mentioned wrist. Then, a mathematical model of the testbed is derived by means of a Lagrangian formulation. The main aim of this model lies in allowing for parameter identification. Finally, the dynamic analysis and frequency response are reported and discussed; these results will play a key role in the parameter identification to be conducted shortly afterwards.

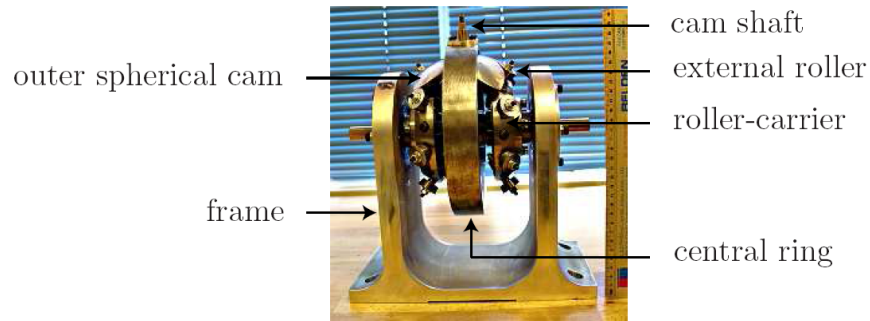


Figure 1: Prototype of the Pitch-Roll Wrist

## 2 TESTBED DESCRIPTION

The pitch-roll wrist testbed, residing in the Robotic Mechanical Systems Laboratory, McGill University, is set up to operate the prototype of the Spherical Epicyclic Cam Train (SECT) and acquire the measured data. The testbed, shown in Fig. 2, whose iconic model is displayed in Fig. 3, is composed of several mechanical parts and electric hardware, namely,

- the *SECT*, which comprises the epicyclic train at the core of the PRW.
- *two torque sensors*, to measure the input shaft torques connected inline with the two servo motors.
- *four couplings*: flexible shaft couplings are used to connect the two motors, torque sensors, and the SECT input shafts.
- the *load and its counterweight*: a gripper is used as a load, and a counterweight, diametrically opposite to the gripper, is provided for static balancing.
- *two brushless servomotors, the amplifier and the data-acquisition system*, which consists of a Digital/Analog (D/A) convertor.

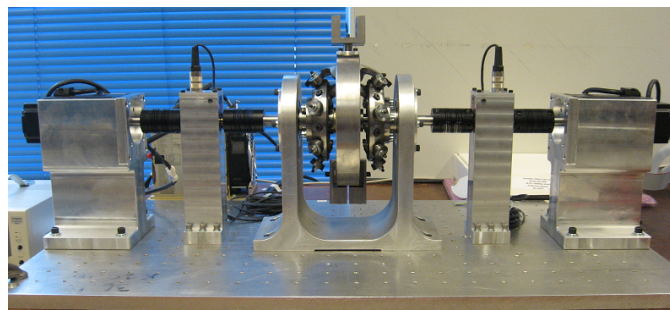


Figure 2: Pitch-Roll Wrist testbed

The electric hardware setup involves torque sensors, a host computer and all needed I/O devices. A host computer with the Windows XP operating system is used to drive the servomotors and

to communicate with the data-acquisition system. The latter, supplied by Quanser Consulting Inc., consists of hardware, namely, Q8 Hardware-in-the-Loop (HIL) Control Board and the D/A Converter Card, as well as software, namely, the Quanser Control Platform. The latter is controlled by QuaRC, which is a multi-functional rapid control development and deployment environment, and is readily integrated with MATLAB Simulink. QuaRC can communicate via the Internet, allowing the user to download controllers anywhere and control them from a remote location, change the control parameters while the controller runs, plot real-time data and save them directly into a MATLAB workspace or file.

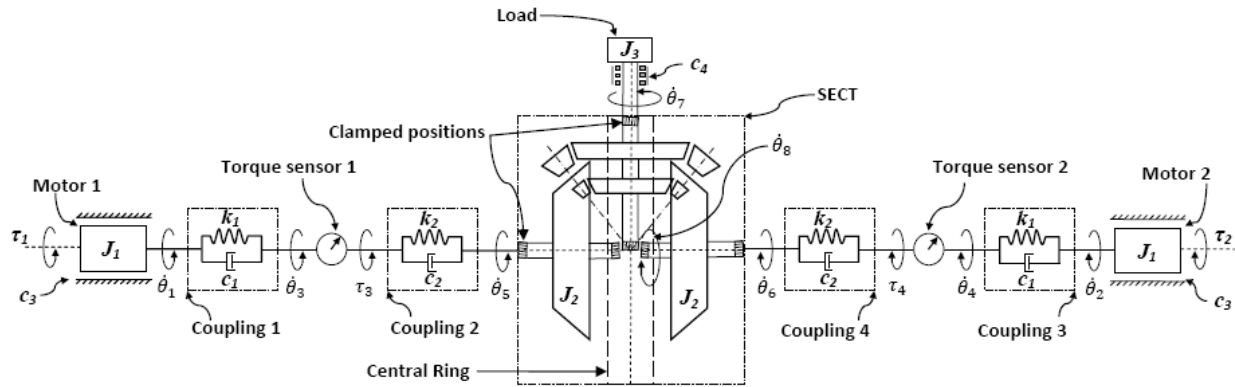


Figure 3: Iconic model of the Pitch-Roll Wrist testbed

### 3 MODEL DEVELOPMENT

In developing the mathematical model for the PRW testbed described above, the Lagrange formulation is adopted. The transfer matrix of the output velocity to the input velocity is derived based on the iconic model of the testbed.

#### 3.1 Iconic Model of the Testbed and Assumptions

In the iconic model of the testbed, illustrated in Fig. 3, the hatched sections are shown as clamped positions where the shafts are held by bearings. The shaft carrying the gripper is mounted and clamped by two bearings located at the centre and the edge of the central ring. The notation adopted is listed here.

$k_1$ : torsional stiffness of couplings 1 and 3

$k_2$ : torsional stiffness of couplings 2 and 4

$c_1$ : coefficient of torsional viscous damping of couplings 1 and 3 (this also takes into account the damping present in the roller bearings of the two motors)

$c_2$ : coefficient of torsional viscous damping of couplings 2 and 4

$c_3$ : coefficient of viscous torsional damping of the load upon rolling (this takes into account the damping present in the roller bearings at the clamped positions)

- $J_1$ : moment-of-inertia of motors 1 and 2
- $J_2$ : combined moment-of-inertia of the roller-carrier, the rollers and attached shafts
- $\mathbf{I}_L$ : combined moment-of-inertia matrix of the cam shaft, the central cam-carrier ring, gripper and conjugate spherical cams
- $\dot{\theta}_1, \dot{\theta}_2$ : angular velocities of motors 1 and 2, respectively
- $\dot{\theta}_3$ : angular velocity of the shaft between couplings 1 and 2
- $\dot{\theta}_4$ : angular velocity of the shaft between couplings 3 and 4
- $\dot{\theta}_5, \dot{\theta}_6$ : angular velocities of the two input shafts
- $\dot{\theta}_7, \dot{\theta}_8$ : rolling and pitching angular velocities of the output cam shaft
- $\tau_1, \tau_2$ : torques measured by the sensors on the input shafts of the SECT

The double output of the SECT, rolling and pitching angular velocities  $\dot{\theta}_7$  and  $\dot{\theta}_8$ , is a function of the two angular velocities of the input shafts,  $\dot{\theta}_5$  and  $\dot{\theta}_6$ . The input-output relation of the SECT is [7]

$$\begin{bmatrix} \dot{\theta}_7 \\ \dot{\theta}_8 \end{bmatrix} = \begin{bmatrix} 1/2 & 1/2 \\ N/2M & -N/2M \end{bmatrix} \begin{bmatrix} \dot{\theta}_5 \\ \dot{\theta}_6 \end{bmatrix} \quad (1)$$

where  $M$  ( $= 4$ ) is the number of lobes of the spherical cams and  $N$  ( $= 7$ ) is the number of rollers on each side of the roller-carrying plates of the SECT. Firstly, we assume that all shafts, connectors, cams and loads are rigid bodies, and all bodies of the SECT are lumped in three rigid bodies, namely, the two input plates together with their rollers and the combination of the central ring together with the cam shaft and gripper. Then, all springs and dashpots are assumed to operate within their linear range. Finally, the composite body of the cam-shaft-gripper-ring is assumed to be statically balanced with its centre of mass located at the intersection  $O$  of the axes of pitching and rolling, based on the design of the SECT, the gripper and the counterweight.

### 3.2 Derivation of the Mathematical Model

We formulate the governing equations using a Lagrangian approach [8]. If we let  $\mathbf{q}$  be the vector of independent generalized coordinates, then, the Lagrange equation of the system is given below:

$$\frac{d}{dt} \left( \frac{\partial L}{\partial \dot{\mathbf{q}}} \right) - \frac{\partial L}{\partial \mathbf{q}} = \frac{\partial(\Pi - \Delta)}{\partial \dot{\mathbf{q}}} \quad (2)$$

where

$L$ : the Lagrangian of the system, given by  $L = T - V$

$T$ : the total kinetic energy of the system

$V$ : the total potential energy of the system

$\Pi$ : the power supplied to the system by force sources

$\Delta$ : the Rayleigh dissipation function associated with all the dashpots in the system

$\mathbf{q}$ : the six-dimensional vector of angular displacements  $\theta_i$ , for  $i = 3, 4, \dots, 8$

Notice that the two angular velocities  $\dot{\theta}_1$  and  $\dot{\theta}_2$  of the two motors are specified, which play the role of control variables and hence, are not generalized coordinates. As well, given that the system

is motion-driven, the power  $\Pi$  supplied by force sources vanishes, i.e.,  $\Pi = 0$

. The total kinetic energy is determined as the sum of all the individual kinetic energies of the different components in the system and is given by

$$T = \frac{1}{2}J_1\dot{\theta}_1^2 + \frac{1}{2}J_1\dot{\theta}_2^2 + \frac{1}{2}J_2\dot{\theta}_5^2 + \frac{1}{2}J_2\dot{\theta}_6^2 + \frac{1}{2}\boldsymbol{\omega}_L^T \mathbf{I}_L \boldsymbol{\omega}_L \quad (3)$$

Notice also that the  $3 \times 3$  inertia matrix  $\mathbf{I}_L$  is a constant when referred to a moving frame, with origin at  $O$ , the  $X$ -axis defined as the axis of pitching, the  $Y$ -axis as the axis of rolling, and the  $Z$ -axis formed by the right-hand rule. In this frame,

$$\mathbf{I}_L = \begin{bmatrix} H_3 & 0 & 0 \\ 0 & J_3 & 0 \\ 0 & 0 & K_3 \end{bmatrix}, \quad \boldsymbol{\omega}_L = \begin{bmatrix} \dot{\theta}_7 \\ \dot{\theta}_8 \\ 0 \end{bmatrix} \quad (4a)$$

whence

$$\frac{1}{2}\boldsymbol{\omega}_L^T \mathbf{I}_L \boldsymbol{\omega}_L = \frac{1}{2}H_3\dot{\theta}_7^2 + \frac{1}{2}J_3\dot{\theta}_8^2 \quad (4b)$$

Substituting eq.(4b) in eq.(3) yields

$$T = \frac{1}{2}J_1\dot{\theta}_1^2 + \frac{1}{2}J_1\dot{\theta}_2^2 + \frac{1}{2}J_2\dot{\theta}_5^2 + \frac{1}{2}J_2\dot{\theta}_6^2 + \frac{1}{2}H_3\dot{\theta}_7^2 + \frac{1}{2}J_3\dot{\theta}_8^2 \quad (5)$$

The total potential energy is determined by the elastic elements, while gravity does not intervene, i.e.,

$$V = \frac{1}{2}k_1(\theta_1 - \theta_3)^2 + \frac{1}{2}k_1(\theta_2 - \theta_4)^2 + \frac{1}{2}k_2(\theta_3 - \theta_5)^2 + \frac{1}{2}k_1(\theta_4 - \theta_6)^2 \quad (6)$$

The Rayleigh dissipation function associated with the system stems from the viscous damping present, which is

$$\Delta = \frac{1}{2}c_1(\dot{\theta}_1 - \dot{\theta}_3)^2 + \frac{1}{2}c_1(\dot{\theta}_2 - \dot{\theta}_4)^2 + \frac{1}{2}c_2(\dot{\theta}_3 - \dot{\theta}_5)^2 + \frac{1}{2}c_2(\dot{\theta}_4 - \dot{\theta}_6)^2 + \frac{1}{2}c_3\dot{\theta}_7^2 + \frac{1}{2}c_3\dot{\theta}_8^2 \quad (7)$$

We have a system with six degrees with freedom,  $\theta_i$ , for  $i = 3, 4, \dots, 8$ , denoting the generalized coordinates. Now, integrating the input-output relation of eq.(1), with respect to time, under the assumption that at initial conditions (i.e., at  $t = 0$ ) all terms vanish, we notice that, out of the six generalized coordinates, only four are independent. Hence, the system has, in fact, four degrees of freedom. Under these conditions, we substitute eqs.(5)–(7) into eq.(2), the Lagrange equation then leading to

$$\mathbf{M}\ddot{\mathbf{q}} + \Delta\dot{\mathbf{q}} + \mathbf{K}\mathbf{q} = \mathbf{f}(t) \quad (8)$$

where  $\mathbf{q}$  is the four-dimensional vector of generalized coordinates and  $\mathbf{f}(t)$  is the four-dimensional vector of input generalized force, namely,

$$\mathbf{q} = \begin{bmatrix} \theta_3 \\ \theta_4 \\ \theta_5 \\ \theta_6 \end{bmatrix}, \quad \mathbf{f}(t) = \begin{bmatrix} c_1\dot{\theta}_1 + k_1\theta_1 \\ c_1\dot{\theta}_2 + k_1\theta_2 \\ 0 \\ 0 \end{bmatrix}$$

Furthermore,  $\mathbf{M}$ ,  $\mathbf{\Delta}$  and  $\mathbf{K}$  are the  $4 \times 4$  mass, damping and stiffness matrices, respectively, namely,

$$\mathbf{M} = \begin{bmatrix} 0 & 0 & 0 & 0 \\ 0 & 0 & 0 & 0 \\ 0 & 0 & J_2 + H_3/4 + J_3 N^2/4M^2 & H_3/4 - J_3 N^2/4M^2 \\ 0 & 0 & H_3/4 - J_3 N^2/4M^2 & J_2 + H_3/4 + J_3 N^2/4M^2 \end{bmatrix}$$

$$\mathbf{\Delta} = \begin{bmatrix} c_1 + c_2 & 0 & -c_2 & 0 \\ 0 & c_1 + c_2 & 0 & -c_2 \\ -c_2 & 0 & c_2 + c_3/4 + c_3 N^2/4M^2 & c_3/4 - c_3 N^2/4M^2 \\ 0 & -c_2 & c_3/4 - c_3 N^2/4M^2 & c_2 + c_3/4 + c_3 N^2/4M^2 \end{bmatrix}$$

$$\mathbf{K} = \begin{bmatrix} k_1 + k_2 & 0 & -k_2 & 0 \\ 0 & k_1 + k_2 & 0 & -k_2 \\ -k_2 & 0 & k_2 & 0 \\ 0 & -k_2 & 0 & k_2 \end{bmatrix}$$

### 3.3 State-Space Representation

A state-space representation as a multiple-input-multiple-output (MIMO) system is derived below, its transfer functions being derived in the sequel. In order to represent the mathematical model in state-space, we first reduce the model given by eq.(8) to a two-dimensional second-order definite system coupled with a two-dimensional first-order system. To this end, matrices and vectors are partitioned as,

$$\mathbf{M} = \begin{bmatrix} \mathbf{O} & \mathbf{O} \\ \mathbf{O} & \mathbf{M}_{II} \end{bmatrix}, \quad \mathbf{\Delta} = \begin{bmatrix} \mathbf{C}_I & \mathbf{C}_{I,II} \\ \mathbf{C}_{I,II}^T & \mathbf{C}_{II} \end{bmatrix}, \quad \mathbf{K} = \begin{bmatrix} \mathbf{K}_I & \mathbf{K}_{I,II} \\ \mathbf{K}_{I,II}^T & \mathbf{K}_{II} \end{bmatrix}$$

$$\mathbf{q} = \begin{bmatrix} \mathbf{q}_I \\ \mathbf{q}_{II} \end{bmatrix}, \quad \mathbf{q}_I = \begin{bmatrix} \theta_3 \\ \theta_4 \end{bmatrix}, \quad \mathbf{q}_{II} = \begin{bmatrix} \theta_5 \\ \theta_6 \end{bmatrix}$$

$$\mathbf{f}(t) = \begin{bmatrix} \mathbf{f}_I \\ \mathbf{0} \end{bmatrix}, \quad \mathbf{f}_I = \mathbf{F}\mathbf{u}, \quad \mathbf{F} = \begin{bmatrix} \mathbf{K}_{1,in} & \mathbf{C}_{1,in} \end{bmatrix}$$

$$\mathbf{K}_{1,in} = \begin{bmatrix} k_1 & 0 \\ 0 & k_1 \end{bmatrix}, \quad \mathbf{C}_{1,in} = c_1 \mathbf{1}, \quad \mathbf{u} = \begin{bmatrix} \theta_{in} \\ \dot{\theta}_{in} \end{bmatrix}, \quad \theta_{in} = \begin{bmatrix} \theta_1 \\ \theta_2 \end{bmatrix}$$

where we define  $\mathbf{0}$  as the two-dimensional zero vector,  $\mathbf{O}$  as the  $2 \times 2$  zero matrix,  $\mathbf{1}$  as the  $2 \times 2$  identity matrix, and all blocks being of  $2 \times 2$ . Then, the mathematical model is rewritten using the above partitioned matrices and vectors.

Regarding the system output, we have torques  $\tau_1$  and  $\tau_2$  as measured quantities. Analyzing the equilibrium of the free-body diagrams of couplings 1 and 3 shown in Fig. 3, we obtain,

$$\tau_1 = k_1(\theta_3 - \theta_1) + c_1(\dot{\theta}_3 - \dot{\theta}_1) \quad (9a)$$

$$\tau_2 = k_1(\theta_4 - \theta_2) + c_1(\dot{\theta}_4 - \dot{\theta}_2) \quad (9b)$$

Thus, the output torques can be expressed as,

$$\boldsymbol{\gamma} = \begin{bmatrix} \tau_1 \\ \tau_2 \end{bmatrix} = \mathbf{K}_{1,in} \mathbf{q}_I + \mathbf{C}_{1,in} \dot{\mathbf{q}}_I - \mathbf{f}_I \quad (10)$$

Proceeding with the state-space representation, the state-variable vector  $\mathbf{x}$  and the output-variable vector  $\mathbf{y}$  are

$$\mathbf{x} = [\mathbf{q}_I, \mathbf{q}_{II}, \mathbf{v}_{II}]^T \quad \mathbf{y} = [\mathbf{q}_I, \boldsymbol{\theta}_{in}, \boldsymbol{\gamma}]^T$$

where  $\mathbf{y}$  includes only measured variables. Further, the state-space equations of the PRW testbed become

$$\dot{\mathbf{x}} = \mathbf{A}\mathbf{x} + \mathbf{B}\mathbf{u} \quad (11a)$$

$$\mathbf{y} = \mathbf{C}\mathbf{x} + \mathbf{D}\mathbf{u} \quad (11b)$$

where

$$\mathbf{A} = \begin{bmatrix} \mathbf{A}_{11} & \mathbf{A}_{12} & \mathbf{A}_{13} \\ \mathbf{0} & \mathbf{0} & \mathbf{1} \\ \mathbf{A}_{31} & \mathbf{A}_{32} & \mathbf{A}_{33} \end{bmatrix}, \mathbf{B} = \begin{bmatrix} \mathbf{B}_{11} & \mathbf{B}_{12} \\ \mathbf{0} & \mathbf{0} \\ \mathbf{B}_{31} & \mathbf{B}_{32} \end{bmatrix}, \mathbf{C} = \begin{bmatrix} \mathbf{1} & \mathbf{0} & \mathbf{0} \\ \mathbf{0} & \mathbf{0} & \mathbf{0} \\ \mathbf{C}_{31} & \mathbf{C}_{32} & \mathbf{C}_{33} \end{bmatrix}, \mathbf{D} = \begin{bmatrix} \mathbf{0} & \mathbf{0} \\ \mathbf{1} & \mathbf{0} \\ \mathbf{D}_{31} & \mathbf{D}_{32} \end{bmatrix}$$

with

$$\begin{aligned} \mathbf{A}_{11} &= \mathbf{C}_I^{-1} \mathbf{K}_I \\ \mathbf{A}_{12} &= \mathbf{C}_I^{-1} \mathbf{K}_{I,II} \\ \mathbf{A}_{13} &= \mathbf{C}_I^{-1} \mathbf{C}_{I,II} \\ \mathbf{A}_{31} &= -\mathbf{M}_{II}^{-1} (-\mathbf{C}_{I,II}^T \mathbf{C}_I^{-1} \mathbf{K}_I + \mathbf{K}_{I,II}^T) \\ \mathbf{A}_{32} &= -\mathbf{M}_{II}^{-1} (-\mathbf{C}_{I,II}^T \mathbf{C}_I^{-1} \mathbf{K}_{I,II} + \mathbf{K}_{II}) \\ \mathbf{A}_{33} &= -\mathbf{M}_{II}^{-1} (-\mathbf{C}_{I,II}^T \mathbf{C}_I^{-1} \mathbf{C}_{I,II} + \mathbf{C}_{II}) \\ \mathbf{B}_{11} &= \mathbf{C}_I^{-1} \mathbf{K}_{1,in} \\ \mathbf{B}_{12} &= \mathbf{C}_I^{-1} \mathbf{C}_{1,in} \\ \mathbf{B}_{31} &= -\mathbf{M}_{II}^{-1} \mathbf{C}_{I,II}^T \mathbf{C}_I^{-1} \mathbf{K}_{1,in} \\ \mathbf{B}_{32} &= -\mathbf{M}_{II}^{-1} \mathbf{C}_{I,II}^T \mathbf{C}_I^{-1} \mathbf{C}_{1,in} \\ \mathbf{C}_{31} &= \mathbf{K}_{1,in} - \mathbf{C}_{1,in} \mathbf{C}_I^{-1} \mathbf{K}_I \\ \mathbf{C}_{32} &= -\mathbf{C}_{1,in} \mathbf{C}_I^{-1} \mathbf{K}_{I,II} \\ \mathbf{C}_{33} &= -\mathbf{C}_{1,in} \mathbf{C}_I^{-1} \mathbf{C}_{I,II} \\ \mathbf{D}_{31} &= -\mathbf{C}_{1,in} \mathbf{C}_I^{-1} \mathbf{K}_{1,in} - \mathbf{K}_{1,in} \\ \mathbf{D}_{32} &= -\mathbf{C}_{1,in} \mathbf{C}_I^{-1} \mathbf{C}_{1,in} - \mathbf{C}_{1,in} \end{aligned}$$

### 3.4 Derivation of the Transfer Matrix

The transfer matrix is a compact representation of the differential equation describing the influence of the input variables onto the output variables, these variables being expressed as polynomial

Table 1: Simulation Parameters

Parameter	Value
$J_2$	$3.8681291 \times 10^{-3} \text{kgm}^2$
$J_3$	$1.2750004 \times 10^{-2} \text{kgm}^2$
$H_3$	$4.2363841 \times 10^{-2} \text{kgm}^2$
$c_1$	$7.83 \times 10^{-3} \text{Nms/deg}$
$c_2$	$8.35 \times 10^{-3} \text{Nms/deg}$
$c_3$	$6.66 \times 10^{-3} \text{Nms/deg}$
$k_1$	$2.11 \text{Nm/deg}$
$k_2$	$0.76 \text{Nm/deg}$

functions of  $s$ , after Laplace-transforming the input-output differential equation [9]. We take the Laplace transforms of eqs.(11a) and (11b) to obtain

$$s\mathbf{X}(s) = \mathbf{A}\mathbf{X}(s) + \mathbf{B}\mathbf{U}(s) \quad (12a)$$

$$\mathbf{Y}(s) = \mathbf{C}\mathbf{X}(s) + \mathbf{D}\mathbf{U}(s) \quad (12b)$$

Thus, the transfer function  $\mathbf{G}(s)$  is obtained as

$$\mathbf{G}(s) \equiv \frac{\partial \mathbf{Y}(s)}{\partial \mathbf{U}(s)} = \mathbf{C}(s\mathbf{1} - \mathbf{A})^{-1}\mathbf{B} + \mathbf{D} \quad (13)$$

#### 4 SIMULATION AND DYNAMICS ANALYSIS

In order to conduct simulation and analysis of the PRW testbed, the inertial properties of the SECT and all system parameters are required. The mass and the moment of inertia of all composite bodies among the SECT are calculated by means of the Model Analysis tool of Pro/E. The physical system parameters of the model, namely, the stiffness and damping coefficients, will be identified and estimated according to the observed input-output experimental data. Before starting the experiment, these parameters are assumed based on experience, from data taken from a previous similar testbed [10]. All parameters used in the simulation system are recorded in Table. 1.

The simulation system was set up in MATLAB/Simulink according to the proposed mathematical model described in eq.(8). Here, one set of harmonic signals, namely,  $\dot{\theta}_1 = \sin(10\pi)$  and  $\dot{\theta}_2 = \sin(10\pi + \pi) = -\sin(10\pi)$ , was chosen as the excitation of the simulation system. The simulation results, illustrated in Fig. 4, show that the pitching velocity  $\dot{\theta}_7$  remains zero while two input angular velocities,  $\dot{\theta}_1$  and  $\dot{\theta}_2$ , have the same speed and different directions. The PRW thus degenerates into a single-degree-of-freedom transmission.

In order to gain insight into the system, we simply perform the Laplace-transform of the model of eq.(8) by letting

$$\mathbf{f}(t) = \mathbf{F}_u \mathbf{u}_u$$

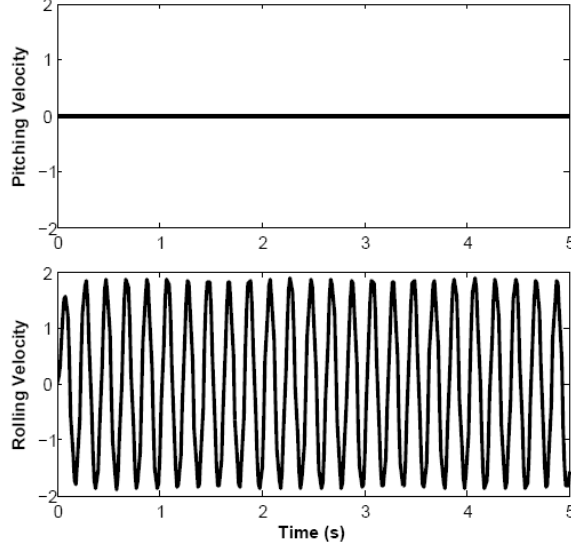


Figure 4: The simulation results under identical motor velocities with opposite signs

with

$$\mathbf{F}_u = \begin{bmatrix} 1 & 0 \\ 0 & 1 \\ 0 & 0 \\ 0 & 0 \end{bmatrix}, \quad \mathbf{u}_u = \begin{bmatrix} c_1 \dot{\theta}_1 + k_1 \theta_1 \\ c_1 \dot{\theta}_2 + k_1 \theta_2 \end{bmatrix}$$

thereby, obtaining

$$(s^2\mathbf{M} + s\mathbf{C} + \mathbf{K})\mathbf{Q}(s) = \mathbf{F}_u\mathbf{U}_u(s) \quad (14)$$

where

$$\mathbf{Q}(s) = \mathcal{L}\{\mathbf{q}(t)\}$$

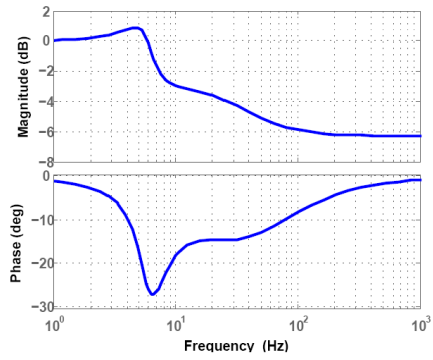
Let

$$\mathbf{U}_u(s) = (c_1s + k_1)\Theta_u(s), \quad \Theta_u(s) = \begin{bmatrix} \Theta_1(s) \\ \Theta_2(s) \end{bmatrix}$$

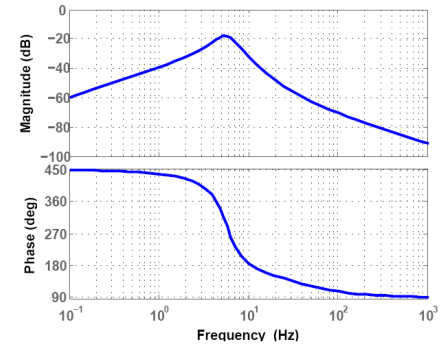
Rearranging terms in eq.(14), to obtain the frequency response of the model, yields

$$\mathbf{H}(s) = \frac{\partial\mathbf{Q}(s)}{\partial\Theta_u(s)} = (s^2\mathbf{M} + s\mathbf{C} + \mathbf{K})^{-1}\mathbf{F}_u(c_1s + k_1) \quad (15)$$

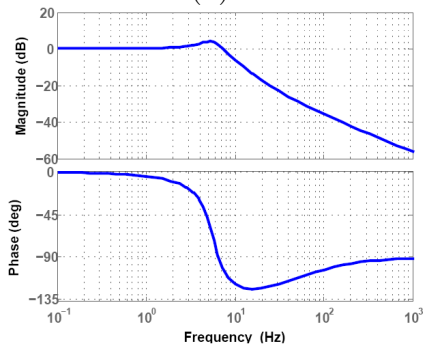
The transfer function turns out to be a  $4 \times 2$  matrix, a total of eight Bode plots thus being obtained. All eight Bode plots are illustrated in Fig. 5, which shows that Figs. 5(a), (b), (c) and (d) are symmetric with Figs. 5(f), (e), (h) and (g), respectively. Notice also that Figs. 5(b), (d), (e) and (g) show a rise in the asymptote, which happens because of the presence of a high pass filter. However, after reaching a pole, the asymptote undergoes a drop of  $-40\text{dB/decade}$ . Moreover, in Figs. 5(c) and (h), we observe that there is a drop of  $-40\text{dB/decade}$ , which produces a net fall of  $-20\text{dB/decade}$ .



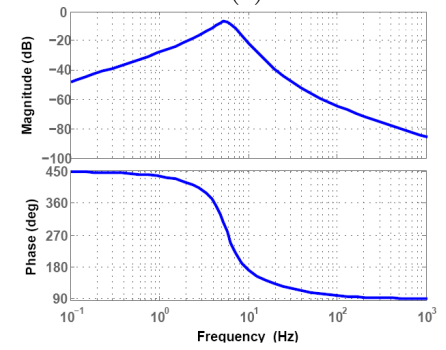
(a)



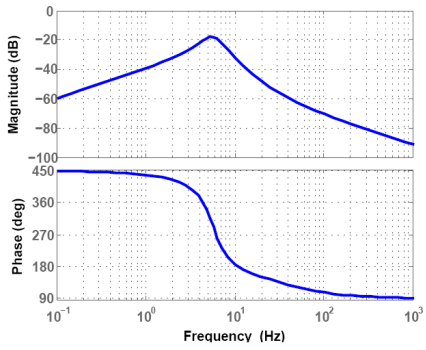
(b)



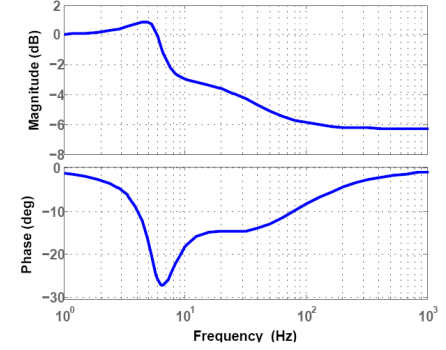
(c)



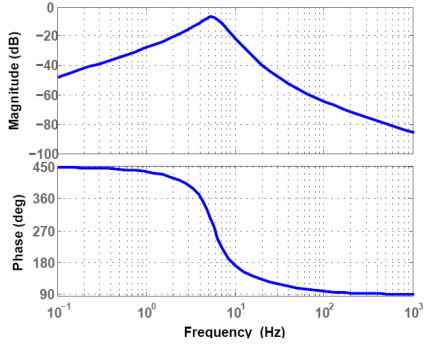
(d)



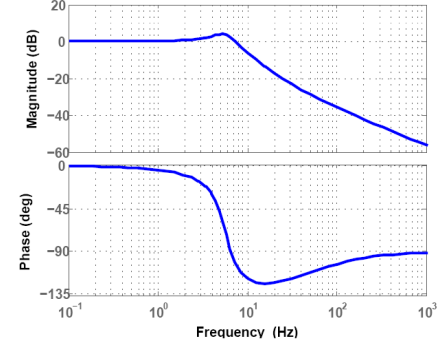
(e)



(f)



(g)



(h)

Figure 5: Bode Plots of (a)  $H_{11}(s)$ ; (b)  $H_{21}(s)$ ; (c)  $H_{31}(s)$ ; (d)  $H_{41}(s)$ ; (e)  $H_{12}(s)$ ; (f)  $H_{22}(s)$ ; (g)  $H_{32}(s)$ ; (h)  $H_{42}(s)$

## 5 CONCLUSIONS

The testbed for a novel mechanical transmission, based on a Spherical Epicyclic Cam Train (SECT), was introduced. This gearless cam-roller transmission is to be used as a robotic wrist to produce pitch and roll, hence the name Pitch-Roll Wrist (PRW). The iconic model of the testbed was produced to develop its mathematical model by means of a Lagrangian approach. Furthermore, the state-space model and the transfer matrix of the testbed system were derived. Finally, the simulation system was set up in MATLAB/Simulink by assuming the values of some system parameters from data available from a similar testbed. Bode plots of the system frequency response were thus obtained. Not surprisingly, the Bode plots reflect the symmetry of the system, which is apparent in Figs. 2 and 3.

## REFERENCES

- [1] Rosheim, M. E., 1989, *Robot Wrist Actuators*, Wiley, New York.
- [2] Tsai, L. W., 1988, "The kinematics of spatial robotic bevel-gear trains," *IEEE J. of Robotics and Automation*, 4(2), pp. 150–156.
- [3] Hsu, C. -H., Chang, C. -C., and Hsu, J. -J., 1999, "Structural synthesis of bevel-gear robotic wrist mechanisms," *Proc. Natl. Sci. Counc. ROC(A)*, 23(4), pp. 518–525.
- [4] Wiitala, J. M. and Stanisic, M. M., 2000, "Design of an overconstrained and dextrous spherical wrist," *ASME J. Mech. Des.*, 122, pp. 347–353.
- [5] Gosselin, C. M. and Caron, F., 1994, "The Agile Eye: a high-performance three-degree-of-freedom camera-orienting device," *IEEE Int. Conf. on Robotics and Auto.*, pp. 781–786.
- [6] Hernandez, S., Bai, S., and Angeles, J., 2006, "The design of a Chain of spherical Stephenson mechanisms for a gearless robotic pitch-roll wrist," *ASME J. Mech. Des.*, 128, pp. 422–429.
- [7] Ma, X. Q., Bai, S. P., Zhang, X. and Angeles, J., 2008, "The design of epicyclic transmissions based on cams and rollers," *Proc. of CSME/SCGM Forum 2008*, Ottawa, Canada, June 5–8.
- [8] Seely, S., 1964, *Dynamic Systems Analysis*, Reinhold Publishing Corporation, New York.
- [9] Savant, C. J. Jr., 1964, *Control System Design*, McGraw-Hill Book Company, New York.
- [10] Song, X., 2002, *The Parameter Identification of a Novel Speed Reducer*, Thesis, Department of Mechanical Engineering, McGill University, Montreal.